TNO report

FEL-97-A069

A comparison on radar range profiles between in-flight measurements and RCS-predictions

TNO Physics and Electronics Laboratory

Oude Waalsdorperweg 63
PO Box 96864
2509 JG The Hague
The Netherlands

Phone +31 70 374 00 00
Fax +31 70 328 09 61

Date

May 1997

Author(s)

R. van der Heiden
L.J. van Ewijk
F.C.A. Groen

DTIC QUALITY INSPECTED 2

Classification

Classified by	:	W. Pelt
Classification date	:	23 April 1997

Title	:	Ongerubriceerd
Managementuittreksel	:	Ongerubriceerd
Abstract	:	Ongerubriceerd
Report text	:	Ongerubriceerd

19970716 174

Copy no	:	9
No of copies	:	29
No of pages	:	28 (excl RDP & distribution list)
No of appendices	:	-

All information which is classified according to Dutch regulations shall be treated by the recipient in the same way as classified information of corresponding value in his own country. No part of this information will be disclosed to any party.

The classification designation Ongerubriceerd is equivalent to Unclassified, Stg. Confidentieel is equivalent to Confidential and Stg. Geheim is equivalent to Secret.
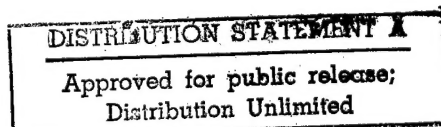
The TNO Physics and Electronics Laboratory is part of TNO Defence Research which further consists of:

TNO Prins Maurits Laboratory
TNO Human Factors Research Institute

Netherlands Organization for
Applied Scientific Research (TNO)

Managementuittreksel

Titel	:	A comparison on radar range profiles between in-flight measurements and RCS-predictions
Auteur(s)	:	Drs. R. van der Heiden, Ir. L.J. van Ewijk, Prof.dr.ir. F.C.A. Groen
Datum	:	mei 1997
Opdrachtnr.	:	A95KM811
IWP-nr.	:	760.2
Rapportnr.	:	FEL-97-A069

Niet-coöperatieve doelclassificatie (NCTR) met radar levert een uitspraak over de identiteit van een vliegtuig. Hiermee vormt NCTR een belangrijke aanvulling op, bijvoorbeeld, het IFF systeem, waarbij het doel actief moet meewerken aan zijn herkenning. Een NCTR techniek die volop in de aandacht staat, is de classificatie van afstandsprofielen. Deze signaturen stellen ééndimensionale radarafbeeldingen van vliegtuigen voor, waarbij de reflectiehaarden van het vliegtuig op de gezichtslijn geprojecteerd zijn. De posities van deze haarden op het vliegtuig zijn karakteristiek voor het *type* vliegtuig, dus is het profiel een belangrijke kandidaat voor vliegherkenning.

Een probleem voor het gebruik van afstandsprofielen voor doelherkenning is de beschikbaarheid van een uitgebreide profielbibliotheek. Meetcampagnes om de bibliotheek te vullen zijn echter duur, tijdrovend en zullen nooit tot een volledige karakterisatie van alle interessante doelen kunnen leiden.

In opdracht van de Koninklijke Marine is vorig jaar een onderzoek van start gegaan waarin wordt onderzocht in hoeverre computermodellen kunnen worden gebruikt voor het *voorspellen* van afstandsprofielen. Deze rekenschema's worden *Radar Cross Section (RCS) prediction techniques* genoemd; de berekende signaturen noemen we *predicties*.

Dit rapport beschrijft de eerste resultaten van een vergelijking tussen profielpredicties en profielmetingen van een complex object. Twee bestanden worden in de vergelijking betrokken. Allereerst een verzameling afstandsprofielen van een gelegenheidsdoel, een Boeing 737-500, gemeten met de FELSTAR radar. Het tweede bestand bevat afstandsprofielen die berekend zijn met het RCS-predictieprogramma RAPPORT, dat op het FEL ontwikkeld is.

Ondanks diverse vereenvoudigingen in zowel het predictieprogramma als het model van de Boeing, is er een redelijke correlatie op voor- en achteraanzichten van het vliegtuig en een vrij goede correlatie op zijaanzichten van het vliegtuig waar te nemen.

Alhoewel hiermee weliswaar een *proof of principle* geleverd is voor het gebruik van RCS-predictietechnieken voor het voorspellen van afstandsprofielen, is voor andere typen vliegtuigen nog niet dezelfde mate van overeenstemming waargenomen.

Lange termijn toekomstig onderzoek zal zich daarom richten op de verbetering van de RCS-predictietechnieken. Op kortere termijn zal worden onderzocht of de predicties voldoende nauwkeurig zijn bij de herkenning van vliegtuigen.

Contents

List of abbreviations

FELSTAR	FEL S-Band Target Acquisition Radar
GO	Geometrical Optics
HRR	High Range Resolution
NCTR	Non-Cooperative Target Recognition
ORFEO	Opbouw van een Rangeprofiel bestand met de FElstar ten behoeve van het Onderzoek naar NCTR (range profile acquisition with the FELSTAR radar for NCTR research)
MRP	Measured Range Profile
PO	Physical Optics
PRP	Predicted Range Profile
RAPPORT	Radar signature Analysis and Prediction by Physical Optics and Ray Tracing
RCS	Radar Cross Section
RRM	Rotational Range Migration
SBR	Shooting and Bouncing Ray

1   Introduction

For a few decades, RCS-prediction techniques have been under development for predicting the total amount of radar reflection of an object at a certain frequency and seen under a particular aspect angle. When the target dimensions are much larger than the wavelength (high-frequency approximation) the combination of *Physical Optics* and *Geometrical Optics* has shown to be a fruitful approach for predicting the RCS of the target [1, 2, 3].

Prediction techniques can be used to compute radar range profiles - these signatures are essentially one-dimensional "images" of aircraft. They are promising candidates for the recognition of targets because they depend on the target geometry [4, 5, 6]. We want to be able to *predict* profiles using an RCS-prediction method and an accurate geometrical description of the target. For future use, predicted profiles can be used to build a target library for aircraft recognition.

This report shows the results of a comparison between predicted range profiles and profiles measured on real, in-flight targets.

The organisation of this report is as follows: in the next section, we will briefly treat high-frequency prediction codes and the implementation that has been chosen for our program, named *RAPPORT*. Section 3 will depict the background of radar range profiles, followed by a description of the range profile acquisition in the subsequent section. Section 5 describes which predictions are made. Subsequently, section 6 shows the comparison between the measurements and the predictions, followed by a discussion in section 7. The final section draws the conclusion.

For the remainder of this report we will use the abbreviations PRP and MRP for 'predicted range profile' and 'measured range profile', respectively.

2   High-frequency RCS-predictions codes

Most high-frequency electromagnetic scattering codes are based on a
combination of *Physical Optics* (PO) and *ray tracing* (related to GO, that is,
Geometrical Optics) as was first suggested by Knott [1] and further described
by Knott *et al* [2] and Zolnick [3].

Methods based on PO and GO can be used in the high frequency region of
electromagnetic scattering. Here, "high frequency" means that the object
needs to be larger than, typically, five wavelengths.

In the Geometrical Optics or GO-approximation it is assumed that the radar
energy propagates along *ray paths*, governed by Fermat's principle. It is
determined which part of the object is visible to the radar and provides the
incident field on an object (ray tracing). If an obstacle is encountered, the
reflected field is determined using the theory of Physical Optics (PO) [7].

The combination of PO and GO also enables us to calculate the scattering
due to *multiple* reflections, likely to occur in corners and cavities [3]. This is
an important property, as these multiple reflections are known to be major
contributors to the total RCS of complex, man-made objects like aircraft,
vehicles and ships.

In case of multiple reflections it is assumed that it suffices to use the PO
approximation for the last reflection only, while for all previous reflections
the waves propagate by the laws of GO. So in the case of multiple reflections,
the incident field is reflected and the direction of the field is calculated with
GO. When the reflected GO field hits the object again, we use it as the
incident field for the second reflection and calculate this contribution to the
RCS with PO if it is not reflected again. We can proceed in the same way to
determine whether triple reflected fields exist and so on, until there are no
reflections left, or until the number of reflections that is chosen for the
computation is reached.

In most techniques the ray-tracing implementation is based upon (a variant
of) the *shooting and bouncing ray* (SBR) technique [8]: a dense grid of rays is
shot from the incident direction towards the target. Rays are traced
according to the law of Geometrical Optics as they bounce around the
target. At the exit point of each ray, a ray tube integration is performed to
sum up its contribution to the total scattered field. A well-known example of
a such a code is XPATCH [9]. The SBR method has the disadvantage that a
sampling density of ten rays per wavelength has to be used to obtain
accurate results.

RAPPORT, acronym for *Radar signature Analysis and Prediction by*

Physical Optics and Ray-Tracing, is an RCS-prediction code developed at TNO-FEL. It is similar to most other high-frequency electromagnetic scattering codes; see Brand [10] for a description.

RAPPORT contains however a fundamental advantage compared to most other codes that lies in the ray-tracing implementation. In RAPPORT the illuminated area on the object is reconstructed explicitly with a certain accuracy, using a non-uniform or *backward* ray tracing algorithm. Once the area is known for a certain aspect angle and object, the RCS can be calculated for any desired frequency. RAPPORT is computationally more efficient than SBR techniques as the ray density to obtain the same accuracy is far less.

The objects used by RAPPORT must be described by a combination of flat polygonal plates. All plates are subdivided into triangular patches called *facets*, with a maximum size that is user controlled. The procedure is to step-wise decrease the patch sizes until convergence is achieved.

The number of multiple reflections that has a significant contribution to the RCS is determined by a similar refinement procedure, i.e., take an increasing number of reflections into account until the total RCS converges.

Features that are not implemented in RAPPORT, but will certainly result in an improved estimate of the actual range profiles, are edge diffraction and the reflection on dielectric materials. Currently, all facets are assumed to be perfectly conducting.

3   Radar range profiles

A range profile can be viewed as a one dimensional "image" of an aircraft, where the parts of the aircraft that reflect the radar radiation, that is, the *scatterers*, are projected onto the line of sight. See figure 3.1.
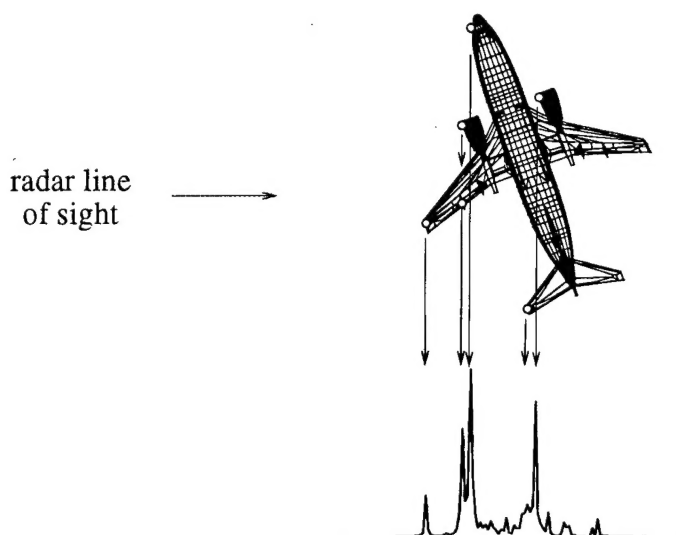
radar line
of sight

Figure 3.1: A range profile of an aircraft viewed from the left hand side. Responses from the aircraft scatterers (circles) are projected onto the line of sight, resulting in a radar range profile (bottom). (Geometrical data by Viewpoint Datalabs International.)

We produced the range profiles by emitting a bandwidth B using N pulses with linearly increasing frequencies, called a *stepped frequency waveform* [11]. The coherent responses (N complex numbers) are, after optional windowing and/or zero-padding, Fourier transformed and from the resulting sequence the phases are discarded – only the magnitudes are considered.

The *target aspect angle* can be expressed as a coordinate pair (α, θ) where α is the *aspect azimuth* and θ is the *aspect elevation*. See figure 3.2. We define the aspect elevation θ as the angle between the radar line of sight and the plane through the wingtips and nose of the aircraft. The elevation is positive if the aircraft is viewed from underneath. We define the aspect azimuth α as the angle between
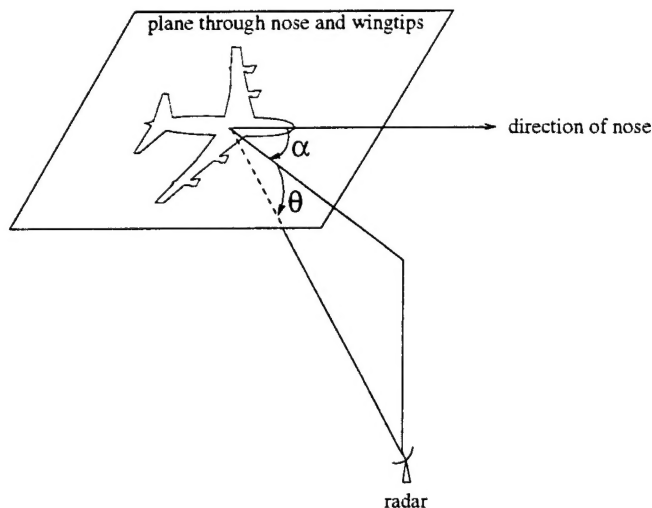
- the direction of the nose of the aircraft and

Figure 3.2: Definition of aspect elevation, θ, and aspect azimuth α. In this particular orientation both α and θ are positive.

- the direction of the radar line of sight projected on the plane through nose and wingtips.

Thus, the aspect azimuth is zero if the aircraft is viewed from nose-on and 180° degrees if viewed from tail-on. Finally, the aspect azimuth is chosen positive if the target is viewed from the starboard side and negative if viewed from the port side. We will assume, however, that the aircraft is symmetric such that a range profile measured at aspect azimuth $-\alpha$ is the same as a range profile measured at α.

The range resolution of a profile can be described in terms of its capability to resolve point targets that are separated in range. The fundamental relationship for the inherent range resolution ΔR associated with radar bandwidth B is [11]

$$\Delta R = \gamma \frac{c}{2B} \tag{3.1}$$

Where c is the speed of light.

Usually, a windowing function is applied before Fourier Transforming to reduce spectral leakage. The price to pay is a reduction in resolution, expressed in the factor $\gamma \geq 1$. For both our measurements and the predictions we applied a Hamming weighting which lowers the first sidelobe to -43 dB. For this window, $\gamma \approx 1.3$.

Range profiles depend strongly on the aspect angle. If an aircraft rotates over a large azimuth angle, such that the outermost scatterers move from

one resolution cell to the other, the measured range profiles during this rotation suffer from *Rotational Range Migration* (RRM) [4].

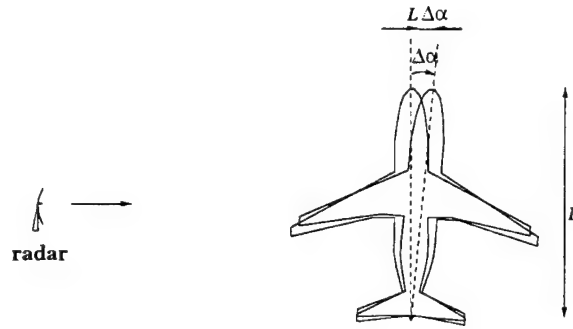See figure 3.3. Suppose we look at an aircraft at broad-side, and consider the

Figure 3.3: The differential path of the outermost scatterers due to a small change in aspect elevation of $\Delta\alpha$ equals $L\Delta\alpha$.

outermost point left (tip of the nose) and right (end of the tail). Let L be the distance between these points. Now, these points do not change their relative position in range over more than a resolution cell if the change in aspect azimuth $\Delta\alpha$ is less than

$$\Delta\alpha < \Delta\alpha_{\mathrm{RRM}} \equiv \frac{\Delta R}{L} \ [\mathrm{rad}] \qquad (3.2)$$

Thus, a range profile measured at (α, θ) does not differ due to Rotational Range Migration from a range profile measured at $(\alpha + \Delta\alpha, \theta)$ if $\Delta\alpha < \Delta\alpha_{\mathrm{RRM}}$.

Rotational range migration also occurs if the aspect *elevation* changes. See figure 3.4. Points on the aircraft that are maximally separated in vertical
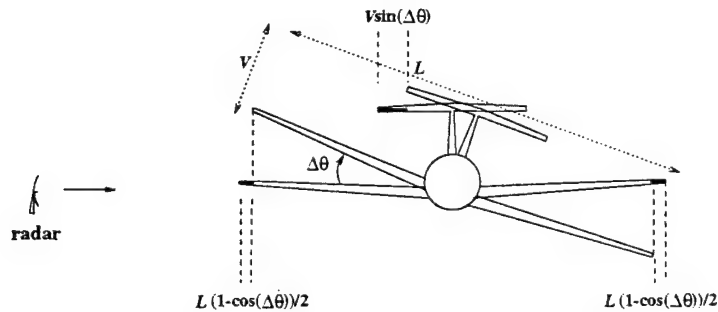

Figure 3.4: Differential path length due to change in aspect elevation. In this geometry, the aircraft has its nose pointed perpendicular on the report (towards the reader) and makes a rotation in elevation of $\Delta\theta$.

direction change their relative path length to the radar with $V \sin(\Delta\theta)$ while rotating over an angle of $\Delta\theta$. Similarly, scatterers that are maximally separated in horizontal direction change their relative path length with $2 \times L(1 - \cos(\Delta\theta))/2$. Note that we have taken the maximum possible separation of scatterers in on the wing tips also equal to L as most civil aircraft, including the target under consideration, are nearly "square". Thus, we may write for the change in aspect elevation $\Delta\theta$ that does not imply a difference due to rotational range migration:

$$\Delta\theta < \Delta\theta_{\text{RRM}} \equiv \min(\arccos(1 - \frac{\Delta R}{L}), \arcsin(\frac{\Delta R}{V})) \ [\text{rad}] \qquad (3.3)$$

Another effect, *speckle*, causes range profile variability for much smaller changes in aspect angle. It is caused when in a single resolution cell two distinct scatterers are present – then, only a slight rotation of the aircraft in aspect azimuth or elevation is enough to change the differential path length to the radar over half the wavelength. This causes the sum of the two scatter contributions to turn from constructive to destructive interference within tiny changes of aspect angle; generally between one and two orders of magnitude smaller than the aspect angle changes associated with Rotational Range Migration.

The effect of speckle is that the amplitudes of the range profile elements may vary rapidly if a sequence of consecutively measured range profiles is considered – the change in aspect angle is due mainly to small aircraft yaw motions during the recording time. The peak positions, however, do not alter.

Thus the following view may be adopted: during the measurement of a sequence of range profiles in real flight, the aircraft rotates with respect to the radar. Over large rotations the profiles decorrelate due to Rotational Range Migration. A small sector may be defined where RRM does not occur, which is called an *RRM-sector*.

It is impossible to measure, and computationally very expensive to predict, range profiles at the dense sampling interval that is required to follow all speckle variations – we would typically need several hundreds of profiles per square degree. We therefore settle for a lower sampling density required to avoid RRM, thereby assuring that the *positions* of the scatterers are well-determined. Then, in the comparison of MRPs with PRPs, it should be kept in mind that the amplitudes of range profile elements that contain multiple scatterers will not be accurately predicted as it cannot be determined precisely what the relative phases of the individual scatterers are. Note, however, that most range-cells will *not* contain multiple scatterers if the resolution is high.

A final remark on the sampling of range profiles in aspect angle is the following: for L and V usually the aircraft length (or wingspan) and the aircraft height are taken. These are, however, the maximum dimensions of the aircraft. Therefore, equations 3.2 and 3.3 usually give a smaller RRM-sector than they will be in reality because radar scatterers are not necessarily present on the outermost parts of the aircraft.

4   In-flight range profile measurements

In this report we consider three legs of fifty range profiles each, acquired in the ORFEO measurement campaign [12] from three different Boeings 737. During the measurements information from a secondary radar was available, which identified the aircraft as a Boeing 737 from either the 300- or the 500 series. The secondary radar uses the same code-name for both series, therefore it is not possible to tell which of the types was actually measured.

The two aircraft types are identical apart from the length of the fuselage, being 33.4 m and 31.0 m for the 300 and the 500 series, respectively. The geometrical model we have available for our comparison is a Boeing 737-500. We are aware, therefore, that the MRP-PRP-correlation may be poorer if the measured target was actually a Boeing 737-300.

The range profiles were measured with the FELSTAR S-band radar located at TNO-FEL in the Hague, the Netherlands. A bandwidth of just over 450 MHz was emitted in 324 steps of 1.4 MHz each.

From these parameters and the maximum target length ($L = 33.4$ m) and height ($V = 11$ m, landing gear stowed) we find that the range resolution is 43 cm, and the aspect angle changes associated with Rotational Range Migration are 0.74 and 2.2 degrees for the aspect azimuth and aspect elevation, respectively. For further details on the measurement procedures, waveform choices and data processing we refer to the ORFEO trials document [12].

The MRPs used in this report were calibrated for system errors, virtually free of influences of radial velocity and acceleration and two-fold oversampled to (partly) reveal spectral contributions that are within grid-points. As mentioned before, the comparison was done on the magnitudes of the profiles only. An MRP thus consists of 648 real numbers.

For each range profile, we estimated the target aspect angle (α, θ) from the tracking data, taking into account the target position, motion and roll-angles. Figure 4.1 shows the aspect angles of the range profiles we use in this comparison. We unfortunately have no firm estimate of the errors in the aspect angle coordinates. The differences in aspect angles will be fairly accurate - a bias on both aspect azimuth and elevation for the whole leg could nevertheless be present. We are confident, however, that the bias for a particular leg will be within 5 degrees for both α and θ.

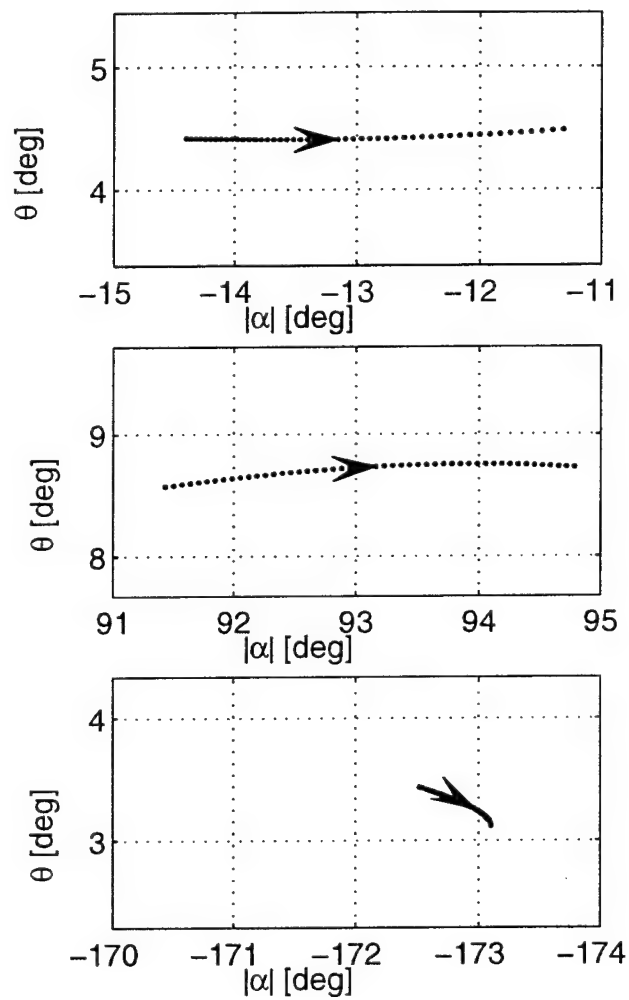Figure 4.2 shows for each of the legs how the aircraft is seen by the radar.

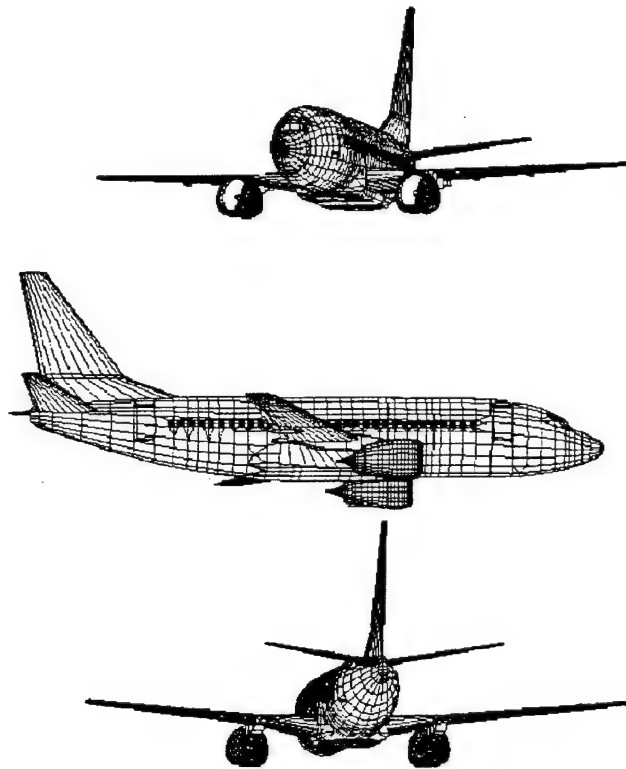*Figure 4.1*: Aspect angles of measured range profiles used in comparison.

Figure 4.2: The Boeing 737-500 model. The topmost figure corresponds to the average viewing angle of leg 1, the second to leg 2 and the third to leg 3. (Geometrical data by Viewpoint Datalabs International.)

5 RAPPORT Range Profile Predictions

The aircraft model used in this report is a commercially available model of a Boeing 737-500 (manufactured by Viewpoint Datalabs International, Orem, Utah, USA); figure 4.2 shows the model at a few aspect angles. The object description compares very well with the real object with respect to the external dimensions. The engines, however, are closed near the front entrance. This will clearly have influence on the computed range profiles, because the engine is a cavity; such structures are known to have a large RCS [3]. Also, there are no arrangements, nor in the model nor in the RCS-prediction code to produce contributions from the rotating parts in the engine.

The geometrical description of the aircraft consists of 8,361 polygons. Subdivision by RAPPORT until convergence was reached, led to an internal geometry description consisting of 27,248 facets. Making the number of reflections larger than three did not add significantly to the total RCS, therefore the maximum number of reflections was chosen to be three.

We used RAPPORT for the prediction at exactly the same 324 frequencies as at which the measurements were performed, and at each of the estimated MRP aspect angles shown in figure 4.1. We thus mimicked the measurement of a stepped frequency waveform. The predicted radar data was processed in the same fashion as the real data, i.e. Hamming weighting, zero-padding, Fourier Transforming and taking the absolute values. We thus produced 150 PRPs.

For a further experiment on leg 2, we computed range profiles on a grid around the estimated aspect angles. As discussed earlier, we settle for a sampling in order to avoid Rotational Range Migration. We chose steps of 0.6 degrees in aspect azimuth and steps of 2.5 degrees in aspect elevation. See figure 5.1.
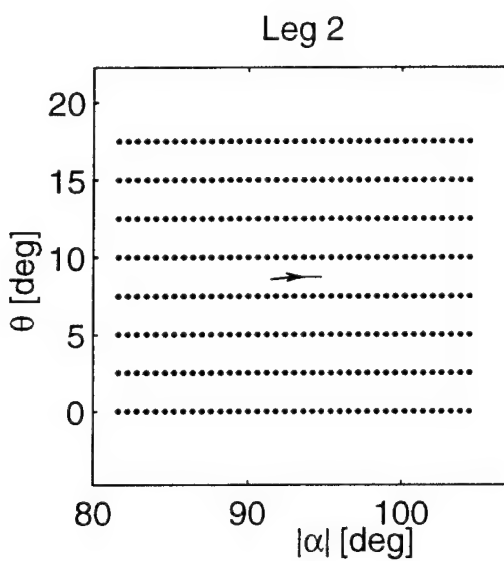
Figure 5.1: Grid at which additional range profiles were computed (dots) around the aspect angles of leg 2 (solid).

6 Comparison results

To quantify the similarity between a predicted and a measured range profile we chose a straightforward measure: the Maximum Correlation Coefficient η. This number is the peak value of of the normalised correlation function. If x is a vector representing the MRP and if y is a vector representing the PRP, this similarity measure is defined as

$$\eta = \max_i(x^{(i)} \cdot y) \qquad (6.1)$$

Here "$\cdot$" denotes the inner product of the two vectors and $x^{(i)}$ is the original vector x, but circularly shifted over i positions to the right. For example, if $x^{(0)} \equiv x = \frac{1}{\sqrt{30}}[1\ 2\ 3\ 4]$ then $x^{(2)} = \frac{1}{\sqrt{30}}[3\ 4\ 1\ 2]$. Both x and y are normalised: it means that the sum of squares of the elements (=total energy) equals one. Therefore, if the PRP and the MRP are identical apart from a discrete shift, η equals unity.

The resulting MRPs and PRPs at the same aspect angles are shown in figure 6.1 in the two topmost diagrams and the bottom left diagram. They show ten measured range profiles (blue), each of them aligned with the predicted profile at the same aspect angle (red). The aircraft contour is aligned with the PRP's. From the fifty profiles we show only the five that have the poorest correlation (the downmost five profiles) and the five that show the best correlation (the topmost five profiles). For all profiles the *magnitudes* are shown. The average Maximum Correlation Coefficients are 0.72, 0.80 and 0.69 for leg 1, 2 and 3, respectively.

Comparing an MRP to a PRP at exactly the same aspect aspect angles disregards the possiblity that there are likely to be errors in the aspect angle estimates of the MRPs. For leg 2 we therefore carried out the following procedure using the PRPs computed at the grid of aspect angles.

1. Shift the entire leg over a chosen angle in both aspect azimuth and aspect elevation.

2. Consider the aspect angle of a shifted MRP. Find the PRP in the grid of aspect angles that is closest in aspect angle.

3. Perform step 2 for all MRPs, such that for each MRP a PRP is found. Note that for several MRPs the same PRP can be found, as neighbouring MRPs differ less in aspect angle than the neighbouring PRPs in the grid.

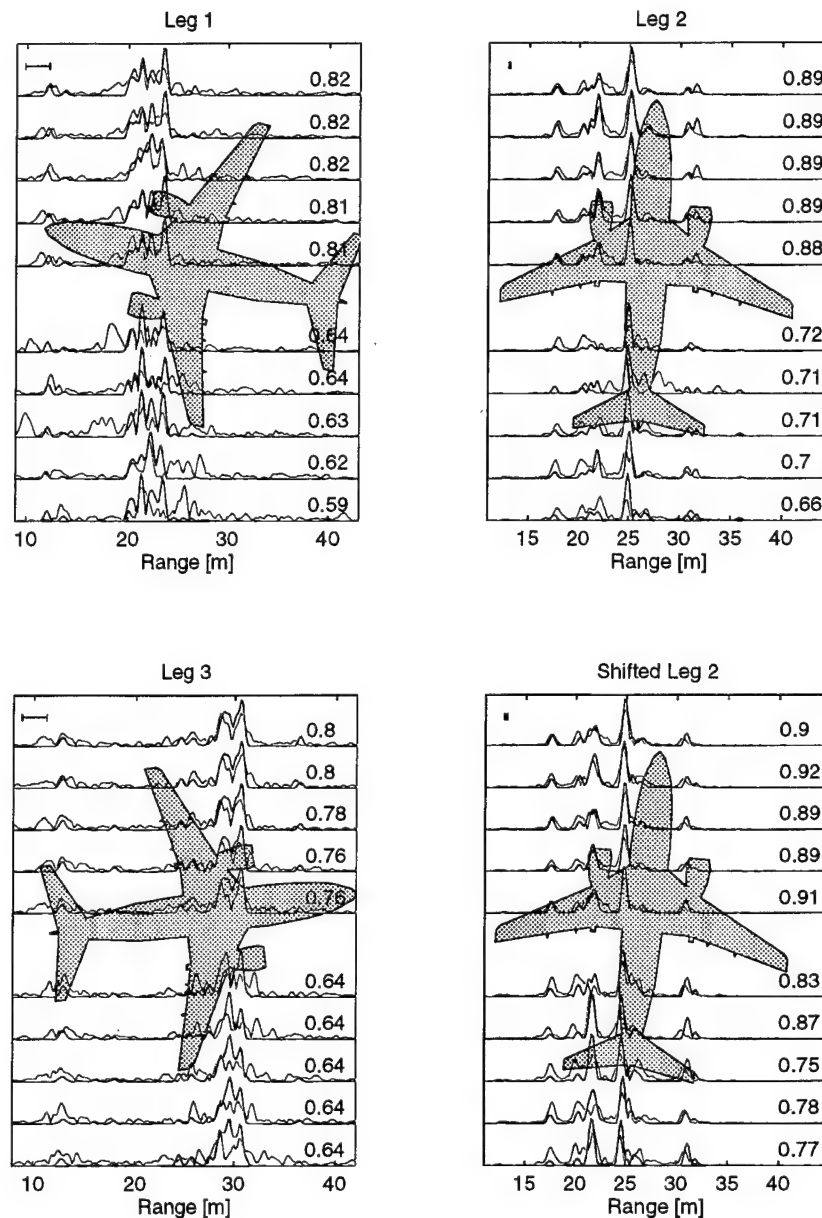4. Compute η for each MRP-PRP pair and average.

Figure 6.1: For each of the three legs ten range profiles are shown. The measurements are blue, the predictions red and the radar is situated at the left-hand side. The numbers in the figures display η. Only the five profiles in the leg with lowest correlation (bottom five) and the five profiles with highest correlation (top five) are displayed. For the two topmost figures and the bottom left figure, the PRP's are computed at the estimated aspect angles. The profiles in the bottom-right show the results of optimal shift from leg 2. In the top-left corner of each figure a bar shows the projected difference in fuselage length between the 300 and 500 series of the Boeing.

If the procedure is repeated for several shifts in aspect azimuth and aspect elevation, figure 6.2 is the result. It shows that the average correlation coefficient increases from 0.80 to 0.85 if a proper shift is chosen. The profiles
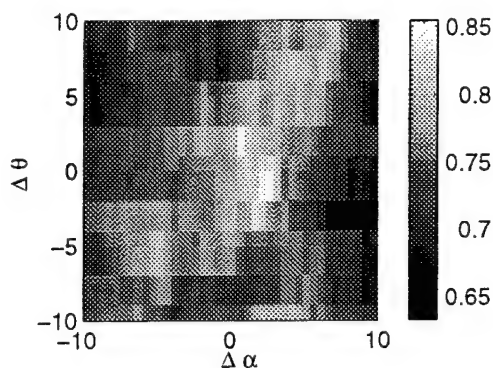

Figure 6.2: Average Maximum Correlation Coefficients $< \eta >$ as function of the shift over aspect azimuth and aspect elevation for leg 2. The maximum $< \eta >$ is found at a shift of $\Delta\alpha = 2.5$ and $\Delta\theta = -2$.

in the bottom right diagram of figure 6.1 show the same ten MRPs of leg 2, but now aligned with profiles that were searched for in the grid. A slightly better match is observed. By matching the leg, we have thus improved the estimate of the target attitude that was found from the radar tracking data.

7   Observations and discussion

1. Viewing figure 6.1 we observe for leg 1 (near nose-on) and for leg 3 (near tail-on) a reasonable agreement between MRPs and PRPs. The correspondence for leg 2 (near-broad side) is much better. Even for the MRP-PRP pairs with lowest η, the correspondence is quite good for leg 2 and still present for leg 3.

    These results are encouraging for the use of RCS-prediction codes for computing radar range profiles of complex targets. At this point, however, we make the remark that the correspondence for this particular aircraft is better than for other aircraft we have available, like the Boeing 747 and the Fokker 100.

2. The correspondence for the broad-side case, leg 3, is clearly favoured by the aspect angle under which we see the aircraft: we do not have reflections from cavities or turbines as we have at head-on and tail-on aspect angles. Also, at these aspect angles not many range cells contain multiple scatterers that give rise to inaccurate amplitudes.

3. For leg 3, we may have actually measured a Boeing 737-300 instead of the somewhat smaller Boeing 737-500 as we do see extra signal in the MRP left from the leftmost scatterer in the PRP.

4. Viewing the same figures again, it is seen that, although the peak positions are quite well predicted, the amplitudes match less well. One of probable causes is speckle: to predict the amplitudes of range cells that contain multiple scatterers, the model and the real target should have the same aspect angle within a few hundredths of a degree.

    Also, the target approximation by small flat patches (instead of round surfaces) and a perfectly conducting surface (instead of dielectric surfaces) is only a first approximation to the actual scattering mechanisms, and is therefore likely to produce inaccuracies in amplitude.

    One of the obvious causes of amplitude mismatch is the normalisation. As no noise-power is present in the PRPs its normalisation pushes the signal components to higher values compared to the MRPs. This is mainly seen in the first and the last leg, where the signal-to-noise ratio of the MRPs is significantly poorer compared to leg 2.

    Another observation is that the spaces between the profile peaks are 'filled' for the MRPs and are much less filled for the PRPs. This influences the amplitudes as the profiles are normalised.

5. Several reflective processes that occur in reality are presently not accounted for in the RCS-prediction code. We mention the modelling of edge-diffraction, creeping waves, cavities and rotating engine parts.

   Possible scatter contributions not modelled on the geometrical model are: antennas, dielectric materials, transitions between dielectric materials, surface roughness, rotating engines and features that differ from aircraft to aircraft from the same type.

   As the results show, for broad-side views the range profiles for this aircraft can be modelled by Physical Optics and Raytracing only. The main difference is that the MRPs have a clear signal component between the main peaks in the profile. For nose-on and tail-on aspect angles, the Physical Optics and Raytracing approximation predicts the most prominent scatterers, but more reflective processes and better models are probably needed to account for the other contributions in the range profile. Presumably, most of the extra non-explained signal in these profiles is due to the engines: cavities and rotating fans and turbines.

   The Boeing 737-500 is powered by the CFM56-3 engine. This high bypass ratio turbofan has an area of the first fan that is much larger than the second one - therefore most of the modulated signal is expected to come from the first fan rather than from the other rotating parts within the engine. To examine whether any discrete responses in the nose-on range profiles are to be expected due to the rotation of this fan, a simple model can be designed where a pointscatterer at the location of the fan is sinusoidally moving back and forth with an amplitude of the thickness of the fan. This thickness, which depends on the distance from the shaft, is typically two wavelengths on S-band. The frequency at which the pointscatterer moves is chosen as the BCF, the *Blade Chopping Frequency*. This quantity corresponds to the rotation of the fan over one blade. For the fan the BCF is approximately 4 KHz.

   Applying this simple model to our waveform we found that, for varying BCF's and fan thicknesses, the contribution from the rotating fan consistently gives an increase of noise level throughout the range profile rather than producing discrete peaks.

   The contributions in the measurements that occur behind the main peaks in the profiles of leg 1 and 3 are therefore probably due to multiple bounces in the engine cavity only. These contributions seem to come from behind the physical engine position as they bounce a few times in the interior before returning to the radar.

6. We also observe that for leg 2 the main features on the aircraft, like the fuselage, the engines and the *flap tracks* (the two dihedral-like

structures on each of the wings) can well be seen in the range profiles.

7. We used the Maximum Correlation Coefficien η as a measure of similarity between MRPs and PRPs. This parameter can however be quite low, even if a correspondence between the peaks is observed. As an example, see figure 6.1, bottom-most profile in the bottom-right figure. For this MRP-PRP pair, a low η is found even though most peaks in the PRP are also present in the MRP. The reason is that η is sensitive to differences in the relative amplitudes of scatterers – these are just the features that are difficult to predict accurately (see point 5). It is therefore of interest to investigate a better measure of similarity that is less sensitive to amplitude. Such a measure will also benefit a future direction of research, the classification of MRPs with PRPs.

8   Conclusion and future work

In this progress report we have demonstrated the proof of principle that for
the Boeing 737 RCS-prediction codes can be used to mimic the measurement
of radar range profiles of a complex target at broad-side aspect angles.

Even though several reflective processes are not included in the prediction
code and the model is a simplified representation of the true target, the
correspondence is convincing.

It means that the ORFEO measurements with the FELSTAR in conjunction
with the use of the secondary radar information resulted in radar range
profiles of good quality. It also showed that the geometrical description of
the model was accurate enough and that the TNO-FEL RCS-prediction code
RAPPORT works well on complex objects.

Nevertheless, preliminary results of current research show that for most
other target types the correspondence is not as evident as for this target.

Long term future work will therefore concern the inclusion of additional
reflective processes into the RCS-prediction code; currently edge diffraction
is being implemented. On a shorter term, we want to find a *measure of
match* between predicted and measured range profiles that performs better
than the used correlation coefficient, because the latter measure depends
crucially on inaccurately predicted peak amplitudes of scatterers in the range
profiles. Such a measure will be very beneficial for a third direction of future
work: the use of predicted range profiles for recognition of measured profiles.
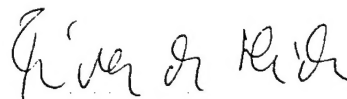
9   References

[1] E.F. Knott.
A tool for predicting the radar cross section of an arbitrary trihedral
    corner.
IEEE SOUTHEASTCON, pages 17–20, April 1981.

[2] E.F. Knott, J.F. Shaeffer, and M.T Tuley.
Radar Cross Section. Its prediction, measurement and reduction.
Artech House inc., 1985.
ISBN 0-89006-174-2.

[3] D.A. Zolnick.
Calculating the radar cross section from multiple-bounce interactions.
In *IEE International Conference on Computation in Electromagnetics*,
    pages 193–196. IEE London, Conference Publication 350, 1991.

[4] S. Hudson and D. Psaltis.
Correlation filters for aircraft identification from radar range profiles.
IEEE Transactions on Aerospace and Electronic systems, 29(3):741–748,
    July 1993.

[5] A. Zyweck and R.E. Bogner.
Radar target classification of commercial aircraft.
IEEE Transactions on Aerospace and Electronic systems, 32(2):598–606,
    April 1996.

[6] H.-J. Li, Y.-D. Wang, and L.-H. Wang.
Matching score properties between range profiles of high-resolution
    radar targets.
IEEE Transactions on Antennas and Propagation, 44(4):444–452, 1996.

[7] G.T. Ruck, D.E. Barrick, W.D. Stuart, and C.K. Krichbaum.
Radar Cross Section Handbook, volume 1.
Plenum Press, New York, 1970.
ISBN 0-306-30343-4.

[8] H. Ling, R. Chou, and S.W. Lee.
Shooting and bouncing rays: calculating the rcs of an arbitrary shaped
    cavity.
IEEE Transactions on Antennas and propagation, 37:194–205, 1989.

[9] D.J. Andersh, M. Hazlett, S.W. Lee, D.D. Reeves, D.P. Sullivan, and
    Y. Chu.
XPATCH: A high-frequency electromagnetic-scattering prediction code
    and environment for complex three-dimensional objects.
IEEE Antennas and Propagation Magazine, 36:65–69, 1994.

[10] M.G.E. Brand.
Radar signature analysis and prediction by physical optics and ray
tracing. The RAPPORT code for RCS prediction.
FEL-95-A097, TNO-FEL, 1995.

[11] D.R. Wehner.
High-Resolution Radar, 2nd edition.
Artech House, 1994.
ISBN 0-89006-727-9.

[12] R. van der Heiden and J. de Vries.
The ORFEO measurement campaign.
FEL-96-A073, TNO FEL, 1996.

10   Signature

H.R. van Es
Group leader

R. van der Heiden
Author

REPORT DOCUMENTATION PAGE
(MOD-NL)

1. DEFENCE REPORT NO (MOD-NL)	2. RECIPIENT'S ACCESSION NO	3. PERFORMING ORGANIZATION REPORT NO
TD97-0103		FEL-97-A069

4. PROJECT/TASK/WORK UNIT NO	5. CONTRACT NO	6. REPORT DATE
25668	A95KM811	May 1997

7. NUMBER OF PAGES	8. NUMBER OF REFERENCES	9. TYPE OF REPORT AND DATES COVERED
28 (excl RDP & distribution list)	12	

10. TITLE AND SUBTITLE

A comparison on radar range profiles between in-flight measurements and RCS-predictions

11. AUTHOR(S)

R. van der Heiden, L.J. van Ewijk, F.C.A. Groen

12. PERFORMING ORGANIZATION NAME(S) AND ADDRESS(ES)

TNO Physics and Electronics Laboratory, PO Box 96864, 2509 JG The Hague, The Netherlands
Oude Waalsdorperweg 63, The Hague, The Netherlands

13. SPONSORING AGENCY NAME(S) AND ADDRESS(ES)

DMKM/WCS/COSPON
Van der Burchlaan 31, 2597 PC The Hague, The Netherlands

14. SUPPLEMENTARY NOTES

The classification designation Ongerubriceerd is equivalent to Unclassified, Stg. Confidentieel is equivalent to Confidential and Stg. Geheim is equivalent to Secret.

15. ABSTRACT (MAXIMUM 200 WORDS (1044 BYTE))

The validation of Radar Cross Section (RCS) prediction techniques against real measurements is crucial to acquire confidence in predictions when measurements are *not* available. In this report we present the results of a comparison on one-dimensional signatures, i.e. radar range profiles. The profiles were measured from a target of opportunity, a Boeing 737. At the same aspect angles and frequencies, profiles were predicted using a high-frequency RCS-prediction code in conjunction with a digitised model of the Boeing. Despite the assumptions and simplifications in both the prediction code and the aircraft model, a reasonable agreement is seen on head-on and tail-on aspect angles. The correspondence on broad-side aspect angles is seen to be better: despite differences in peak amplitudes, normalised correlation coefficients up to 0.9 are observed.

16. DESCRIPTORS	IDENTIFIERS
Radar cross section	Physical optics
Radar	Tay tracing
Mathematical model	Radar cross section prediction

17a. SECURITY CLASSIFICATION (OF REPORT)	17b. SECURITY CLASSIFICATION (OF PAGE)	17c. SECURITY CLASSIFICATION (OF ABSTRACT)
Ongerubriceerd	Ongerubriceerd	Ongerubriceerd

18. DISTRIBUTION AVAILABILITY STATEMENT	17d. SECURITY CLASSIFICATION (OF TITLES)
Unlimited Distribution	Ongerubriceerd

Distributielijst

1.   Bureau TNO Defensieonderzoek
2.   Directeur Wetenschappelijk Onderzoek en Ontwikkeling*)
3.   HWO-KL*)
4.   HWO-KLu*)
5.   HWO-KM
6.   HWO-CO*)
7 t/m 9.   KMA, Bibliotheek
10.   DMKM/WCS/HCOSPON, Drs. W. Pelt
11.   DMKM/WCS/EMDC
12.   Marstaf/OBS
13.   KIM, vakgroep E
14.   DMKL/AT&WO, t.a.v. Ir. N. Pos
15.   DMKLu/MXS
16.   ANCP 1.30, t.a.v. Dr. P.N.R. Stoyle, Defence Research Agency
17.   Directie TNO-FEL, t.a.v. Dr. J.W. Maas
18.   Directie TNO-FEL, t.a.v. Ir. J.A. Vogel, daarna reserve
19.   Archief TNO-FEL, in bruikleen aan M&P*)
20.   Archief TNO-FEL, in bruikleen aan Ir. C. Eberwijn
21.   Archief TNO-FEL, in bruikleen aan Ir. H.R. van Es
22.   Archief TNO-FEL, in bruikleen aan Ir. G.A. van der Spek
23.   Archief TNO-FEL, in bruikleen aan Ir. A.G. Huizing
24.   Archief TNO-FEL, in bruikleen aan Ir. H.J.M. Heemskerk
25.   Archief TNO-FEL, in bruikleen aan Drs. R. van der Heiden
26.   Archief TNO-FEL, in bruikleen aan Ir. L.J. van Ewijk
27.   Archief TNO-FEL, in bruikleen aan Prof.dr.ir. F.C.A. Groen
28.   Documentatie TNO-FEL
29.   Reserve

            TNO-PML, Bibliotheek**)
            TNO-TM, Bibliotheek**)
            TNO-FEL, Bibliotheek**)